International Journal of Nanomedicine

Dovepress
open access to scientific and medical research

Open Access Full Text Article

ORIGINAL RESEARCH

pH-Responsive Artesunate Polymer Prodrugs with Enhanced Ablation Effect on Rodent Xenograft Colon Cancer

This article was published in the following Dove Press journal:
International Journal of Nanomedicine

Dan-Li Hao
Ran Xie
Ge-Jing De
Hong Yi
Chen Zang
Mi-Yi Yang
Li Liu
Hai Ma
Wei-Yan Cai
Qing-He Zhao
Feng Sui
Yan-Jun Chen

Institute of Chinese Materia Medica, China Academy of Chinese Medical Sciences, Beijing 100700, People's Republic of China

Purpose: In this study, pH-sensitive poly(2-ethyl-2-oxazoline)-poly(lactic acid)-poly(β-amino ester) (PEOz-PLA-PBAE) triblock copolymers were synthesized and were conjugated with an antimalaria drug artesunate (ART), for inhibition of a colon cancer xenograft model.

Methods: The as-prepared polymer prodrugs are tended to self-assemble into polymeric micelles in aqueous milieu, with PEOz segment as hydrophilic shell and PLA-PBAE segment as hydrophobic core.

Results: The pH sensitivity of the as-prepared copolymers was confirmed by acid-base titration with p*K*b values around 6.5. The drug-conjugated polymer micelles showed high stability for at least 96 h in PBS and 37°C, respectively. The as-prepared copolymer prodrugs showed high drug loading content, with 9.57%±1.24% of drug loading for PEOz-PLA-PBAE-ART4. The conjugated ART could be released in a sustained and pH-dependent manner, with 92% of released drug at pH 6.0 and 57% of drug released at pH 7.4, respectively. In addition, in vitro experiments showed higher inhibitory effect of the prodrugs on rodent CT-26 cells than that of free ART. Animal studies also demonstrated the enhanced inhibitory efficacy of PEOz-PLA-PBAE-ART2 micelles on the growth of rodent xenograft tumor.

Conclusion: The pH-responsive artesunate polymer prodrugs are promising candidates for colon cancer adjuvant therapy.

Keywords: artesunate, micelles, pH responsive, polymer prodrug, poly(2-ethyl-2-oxazoline), poly(β-amino ester)

Introduction

Colon cancer was regarded as one of the most common malignancies with high mobidity and mortality worldwide, with estimated 1.1 million new cases and 551,269 deaths in 2018 worldwide,[1] which posted great challenges to human life and health. Currently, the mainstream clinical treatments for cancer are surgery, chemotherapy, and radiotherapy, etc.[2] Among which chemotherapy was considered as one of the main therapies for colon cancer.[3] However, the prognosis of chemotherapy is hardly optimistic due to the non-targeted anti-cancer drug delivery to the tumor site and the severe toxic effects on normal tissues, leading to limited therapeutic efficacy as well as drug resistance and/or migration of the tumor cells to other organs, thus limiting the 5-year survival rates of patients.[4] Therefore, it is urgent to develop novel drug delivery depots with tumor-specific drug delivery characteristics and less toxic side effects on normal tissues.[5]

Artesunate (ART), a semi-synthetic derivative of artemisinin,[6] has been recognized as a safe and highly effective anti-malaria drug.[7] In recent years numerous

Correspondence: Qing-He Zhao; Yan-Jun Chen
Tel/Fax +86-10-84036059
Email qhzhao@icmm.ac.cn; yjchen@icmm.ac.cn

http://doi.org/10.2147/IJN.S242032

studies have revealed its anti-tumor effect on various cancer cell lines,[8] including multiple myeloma,[9] chronic myeloid leukemia,[10] bladder cancer,[11] breast cancer,[12] head and neck tumor,[13] hepatocellular carcinoma,[14] prostate cancer,[15] and colon cancer,[16] etc. Several in vitro studies revealed that ART can induce the pleiotropic responses in cancer cells, including inhibition of cell proliferation via cell cycle arrest,[17] apoptosis,[18] induction of DNA lesions,[19] anti-angiogenesis,[20] and modulation of nuclear receptor responsiveness, etc. In addition, it has been reported that artesunate exhibited promising advantages for treatment of tumor, such as the selective inhibition effect on multiple tumor cells, and less toxicity toward healthy tissues.[8] ART was also employed in combination with other anticancer agents for synergistic therapy of cancer.[21] However, the applications of artesunate in clinic are still limited due to its poor water solubility, short half-life in blood circulation, low bioavailability, as well as poor stability. Therefore, it is highly desirable to design an ART depot with sustained release and targeted delivery properties to further explore its applications in other indications such as tumor therapy.

Nanoscale drug delivery systems (NDDS) using liposomes, polymer micelles and nanoparticles, etc., have been extensively investigated for targeted delivery of chemotherapeutic drugs in the treatment of cancer due to their enhanced permeability and retention (EPR) effect on tumor malignancies. Bu reported pH and reduction dual-responsive micelles to deliver doxorubicin (DOX), which showed excellent performances in delivering DOX under pH and redox stimuli.[22] NDDS can also offer improved pharmacokinetic properties, controlled and sustained release of drugs, and more importantly, lower systemic toxicity. A variety of nanotechnology has been developed in the past years to improve the solubility and bioavailability of ART.[23–26] ART loaded liposomes were reported with glioma targeting capabilities with enhanced toxicity towards glioma U87 cells.[27] Jin et al reported artesunate nanoliposomes, prepared with cholesterol and an appropriate amount of lecithin via thin film hydration method, showing stronger antitumor effect on HepG2 cells than that of free artesunate.[28]

In recent years, stimuli-responsive nanoparticles, from which the drug release can be triggered by pH, temperature and light, etc., have been intensively investigated as smart drug-delivery systems for various therapeutic applications.[29] Poly(2-ethyl-2-oxazoline) (PEOz) is a hydrophilic polymer with advantageous biocompatibility and water-soluble properties, which has been approved by the Food and Drug Administration (FDA) of the USA with applications in the fields of food, pharmaceuticals, etc.[30] Biomaterials modified with PEOz have shown enhanced circulation half-life, improved tumor accumulation, and reduced off-target effects. Poly-D,L-lactide (PLA) has been applied as a hydrophobic segment in numerous drug delivery systems.[31] Poly(β-amino esters) (PBAE), synthesized by Michael addition reaction using primary or secondary diamines and diacrylates, was extensively used for delivery of drugs and siRNAs due to its pH-responsive properties.[32]

In this study, we prepared pH-sensitive poly(β-amino ester) copolymers with subsequent conjugation with ART to improve the therapeutic efficacy of ART against colon cancer. The drug cargo was constituted of PEOz as hydrophilic corona and polylactide/PBAE as hydrophobic core (Scheme 1). The copolymer exhibited proton sponge properties at pH below its p*K*b (~6.5) owing to the presence of amine groups.[33] The drug-loaded copolymer micelles could be accumulated in tumor tissue owning to the EPR effect.[34] In this work, the pH-responsive prodrug micelles showed enhanced cellular internalization and stronger inhibitory effect on CT-26 cells. Moreover, the ART-conjugated prodrugs were demonstrated with elevated therapeutic efficacy on rodent xenograft tumors, thus highlighting their great potential for applications in the treatment of colon cancer.

Materials and Methods

Materials and Cell Lines

N-Boc-ethanolamine was provided by Ark (Qingyuan, Guangdong, China). Tin (II) 2-ethylhexanoate, and 4′,6-diamidino-2-phenylindole (DAPI) were purchased from Sigma-Aldrich (St. Louis, MO, USA). D,L-lactide was received from Jinan Daigang (Jinan, Shandong, China). 2-Ethyl-2-oxazoline (EOz), 4-toluene sulfonyl chloride, 2-amino-1,3-propanediol, 6-amino-1-hexanol, 1,6-hexanediol diacrylate and 4-dimethylaminopyridine were purchased from Aladdin (Shanghai, China). Acryloyl chloride, 1,4-butanediol diacrylate, 1,9-bis-(acryloyloxy) nonane and coumarin-6 (C_6) were obtained from TCI (Tokyo, Japan). 1-(3-(Dimethylamino) propyl)-3-ethylcarbodiimide hydrochloride was provided by Adamas (Shanghai, China). Artesunate (ART) was purchased from MACKLIN (Shanghai, China). ART injection was obtained from Guilin Nanyao (Guilin, Guangxi, China). 3-(4,5-Dimethylthiazol-2-yl)-2,5-diphenyltetrazolium bromide (MTT) was purchased from Beyotime Biotechnology (Shanghai, China). Fetal bovine serum (FBS), RPMI-1640 medium (RPMI) and trypsin-EDTA were obtained from

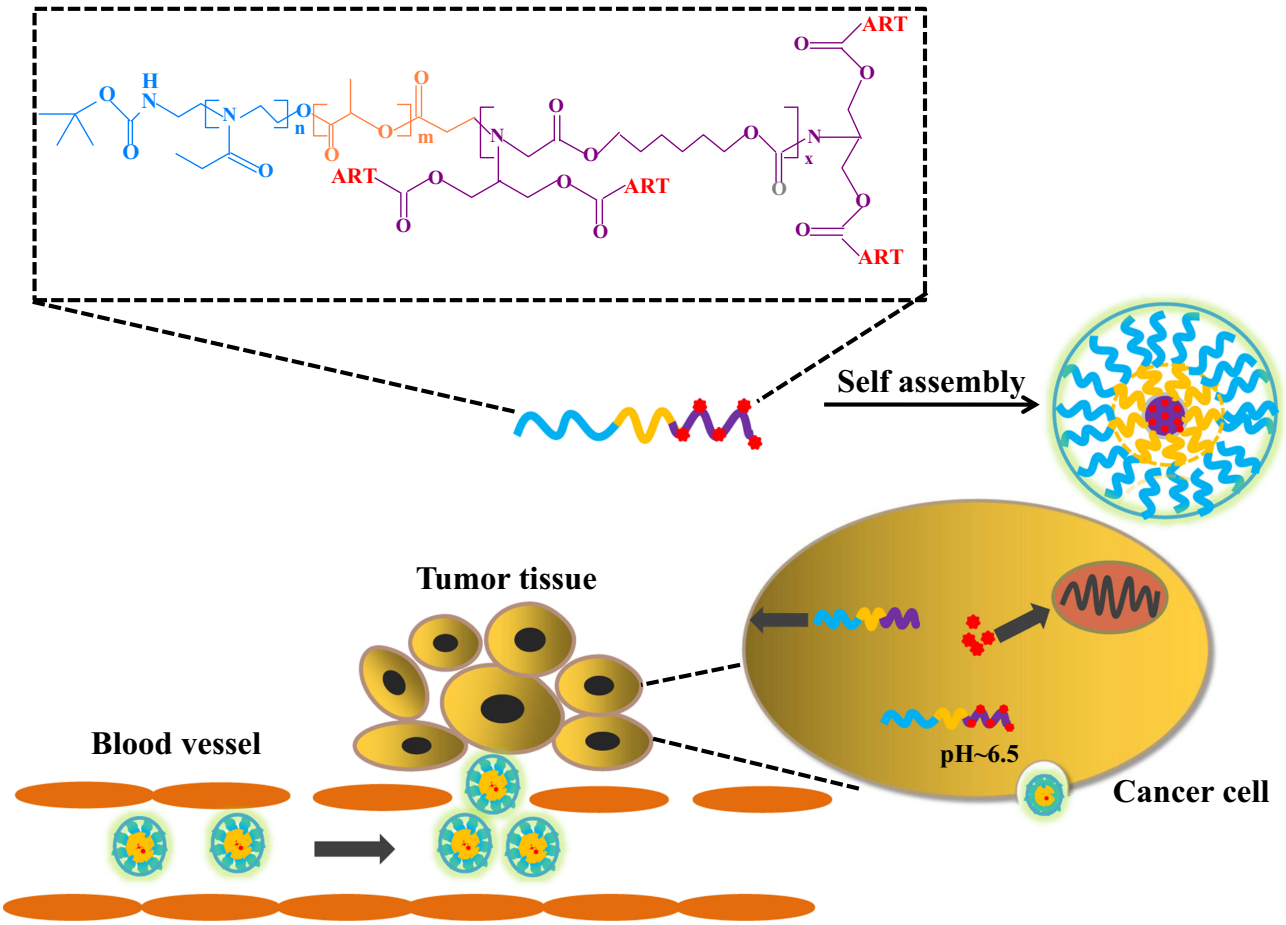

Scheme 1 The formation of polymeric micelles of the PEOz-PLA-PBAE polymer prodrugs and the cellular delivery of the ART-conjugated prodrugs.

Gibco Company (San Diego, CA, USA). All other chemicals were of analytical or HPLC grade and were used as received. Mouse CT-26 colon cancer cells (Shanghai Zhong Qiao Xin Zhou Biotechnology Co, Ltd., Shanghai, China) were used and incubated in RPMI-1640 medium supplemented with 10% FBS and 1% penicillin–streptomycin at 37°C, 5% CO_2 and 95% humidity.

Polymer Synthesis and Characterization

Synthesis of Boc-OTs

Boc-OTs was employed as an initiator and was synthesized by substitution reaction (Scheme 2). In brief, 1.0 g (6.2 mmol) of N-Boc-ethanolamine and 1.73 mL (12.4 mmol) of triethylamine (TEA) were dissolved in 5 mL anhydrous dichloromethane (DCM). After which 1.3 g (6.82 mmol) of 4-toluene sulfonyl chloride was dissolved in 5 mL DCM and was dropwise added into the above solution under ice bath. After 4 hrs of vigorous agitation, the ice bath was removed, and the reaction was allowed to continue for an additional 24 hrs. Then, the product was isolated and purified through silica gel column with petroleum ether as eluent and was precipitated in hexane and vacuum dried to obtain white powder product (Yield 45.6%).

Synthesis of PEOz

PEOz was synthesized by ring-opening polymerization of 2-ethyl-2-oxazoline with Boc-OTs as initiator. Shortly, 1.2 g (3.34 mmol) of Boc-OTs and 30 g (0.30 mol) EOz were dissolved in 100 mL acetonitrile, and the polymerization was conducted at 100°C for 48 h under N_2 protection. The reaction was terminated by addition of 100 mL of 0.1 M KOH methanol solution. Then, the obtained polymer was dialyzed (MWCO = 3500) against deionized water for 2 days, and was lyophilized (Yield 51.3%).

Synthesis of PEOz-PLA

Poly (2-ethyl-2-oxazoline)-*b*-poly(lactide) (PEOz-PLA) was synthesized by ring opening polymerization. Briefly, 1.0 g (6.94 mmol) of D, L-lactide and 1.67 g (0.42 mmol) of PEOz were dissolved in 5 mL anhydrous toluene and were initiated by tin (II) octoate as catalyst at 130°C for 24 h. The

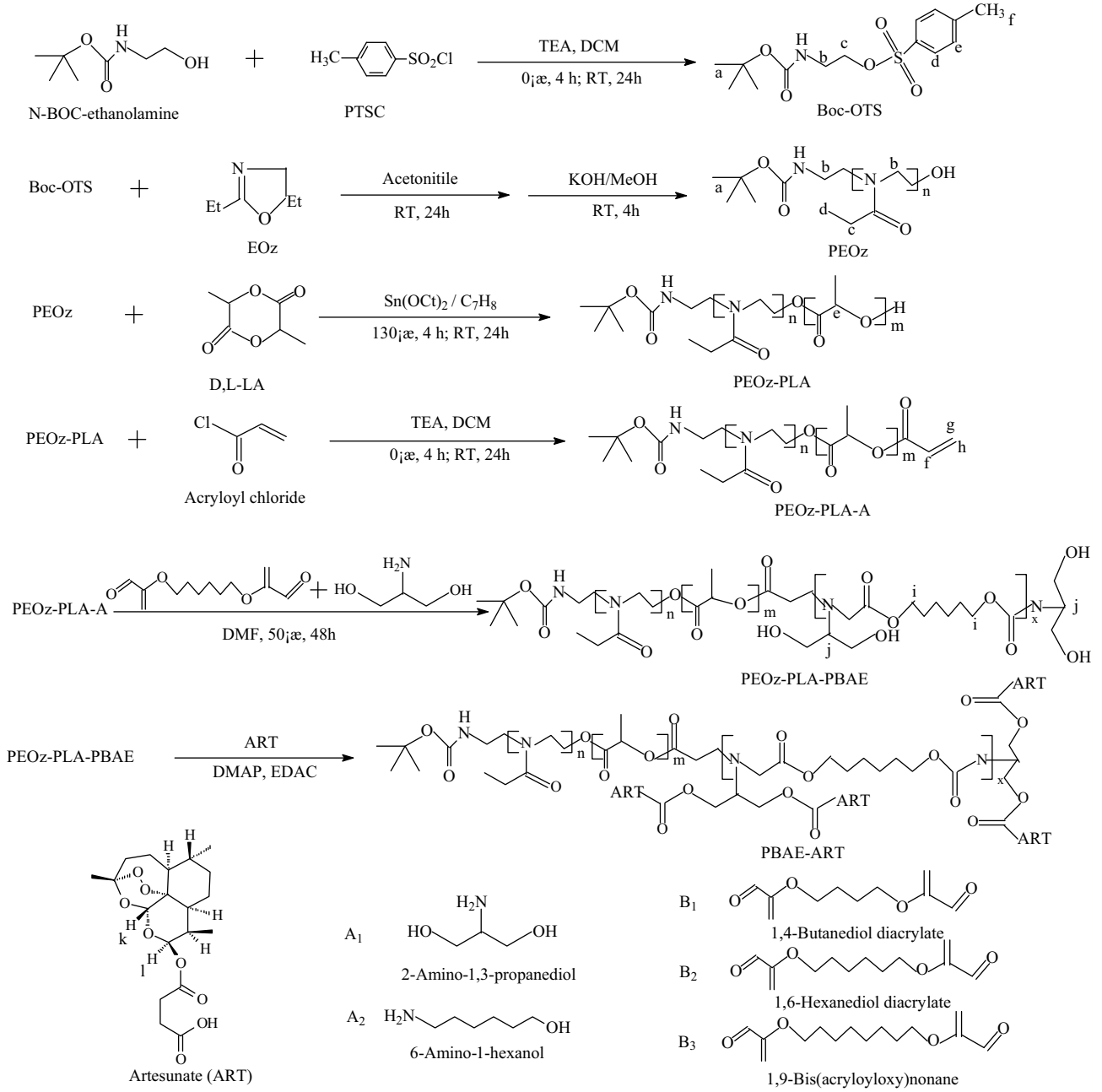

Scheme 2 The synthesis routes and composition of Boc-OTs, PEOz, PEOz-PLA, PEOz-PLA-PBAEs and PBAE-ART prodrugs.

copolymer PEOz-PLA was obtained by precipitation in diethyl ether and vacuum drying. (Yield 85.4%)

Acetylation of PEOz-PLA

To activate the terminal hydroxyl groups of PEOz-PLA, 0.58 g (0.1 mmol) of PEOz-PLA and 28 μL (0.2 mmol) of TEA were dissolved in 5 mL dichloromethane (DCM), and 40.6 μL (0.5 mmol) of acryloyl chloride was added dropwise at 4°C and the reaction was allowed to continue overnight. The solvent was removed via rotary evaporation. The terminal activated PEOz-PLA-A was purified by dissolution/precipitation for 3 times by DCM/diethyl ether and vacuum dried. (Yield 89.6%)

Synthesis of PEOz-PLA-PBAE Triblock Copolymers

A 2.90 g (0.5mmol) of acrylic ester terminated PEOz-PLA -A was dissolved in DCM and reacted with 5 mmol of 1,4-butanediol diacrylate (0.99 g) (or 1,6-hexanediol diacrylate (1.13 g), or 1,9-bis(acryloyloxy) nonane) (1.35 g) and 5.5 mmol of 2-amino-1,3-propanediol (0.501 g) (or

6-amino-1-hexanol (0.645 g)) at 50°C for 24 h. The final product PEOz-PLA-PBAE was obtained by precipitation/dissolution in diethyl ether/DCM thrice and vacuum drying. (Yield 78.4%)

Synthesis of ART-Conjugated Polymeric Prodrug

A 3.63 g (0.5 mmol) of PEOz-PLA-PBAE copolymer and 0.96 g (2.5 mmol) of ART were dissolved in 15 mL DCM, and 0.48 g (2.5 mmol) of 1-(3-(dimethylamino) propyl)-3-ethylcarbodiimide hydrochloride (EDAC) and 0.031 g (0.25mmol) of 4-dimethylaminopyridine (DMAP) were added into the solution to conjugate ART onto the side chains of the copolymer. The solution was stirred at room temperature for 24 h. The solvent was removed by rotary evaporation to terminate the reaction. The copolymer was reconstituted by DMF and placed into dialysis tubing (MWCO = 3500) and dialyzed against deionized water for 2 days. The solution was filtered through 0.22 μm filter and vacuum dried to obtain ART-conjugated prodrugs.

Characterization of Copolymers and Prodrugs

^{1}H NMR spectra of copolymers were obtained by a Bruker Ascend™ 600 MHz NMR spectrometer (Billerica, MA, USA) in $CDCl_3$ at 25°C. The molecular weight of the prodrugs was characterized using gel permeation chromatography (GPC) equipped with a Waters Styrage™ HT3 GPC column (300 mm × 7.8 mm), a Waters 515 HPLC pump and a Waters 2410 refractive index detector. Tetrahydrofuran was used as mobile phase with a flow rate of 1.0 mL/min. Narrow distributed polystyrene was used as calibration standard. The p*K*b values of the as-prepared copolymers were determined by acid/base titration method. In a typical experiment, 20 mg of the polymer was dissolved in 20 mL deionized water and the pH was adjusted to less than 2.0, after that 20 μL of 0.1 N NaOH was added and the solution pH was measured. The p*K*b was plotted as the inflection point of the titration curve. The critical micelle concentration (CMC) of the polymers was determined by fluorescence measurements using pyrene fluorescence spectroscopy according to our previous report.[35] The emission wavelength was set at 390 nm with excitation slit and emission slit of 1.0 nm and 10.0 nm, respectively. The excitation intensities at a wavelength range of 300–360 nm were monitored using a fluorescence spectrophotometer (F-2000, HITACHI, Tokyo, Japan). The concentration of the polymer solution was varied from 5.0×10^{-4} to 1.0 mg/mL containing 6×10^{-8} M of pyrene as a probe. The fluorescence intensity ratio of I_{336}/I_{334} was calculated against polymer concentration to determine the CMC of the respective copolymers.

The size and zeta potential of the as-prepared micelles were measured on a Malvern Zetasizer Nano ZS90 (Worcestershire, United Kingdom) with a detection angle at 90°. TEM images were obtained using a HITACHI H7650 (Tokyo, Japan) transmission electron microscope operated with an acceleration voltage of 80 kV. The samples were prepared by dipping a TEM grid into a 0.1 wt % sample solution. The extra water was blotted with filter paper. The drug grafting ratio (GR) was determined by cleavage of the drug-conjugated polymers with esterase and was subjected to high-performance liquid chromatography (HPLC, Agilent 1260, Santa Clara, CA, USA) equipped with an Agilent C_{18} column (4.6 × 250 mm, 5 mm, column temperature 30°C), with a mobile phase of acetonitrile/water (45:55, v/v) and a flow rate of 1.0 mL/min. A fixed amount of lyophilized micelles was dissolved in methanol and subjected to HPLC and was detected via a UV detector at 216 nm. The content of ART was determined by a calibration curve of ART in the mobile phase. The grafting ratio (GR) was calculated according to the following equation:

$$GR = \frac{\text{weight of ART in the prodrug}}{\text{weight of prodrug}} \times 100\%$$

In Vitro Drug Release

The release of ART from micelles was performed according to a protocol reported previously.[36] In short, 2 mL of ART-conjugated micelles solution was sealed in a dialysis bag (MWCO 3500) and was incubated in 15 mL of phosphate buffered saline (PBS) at pH 7.4 or pH 6.0. The drug release was carried out at 37°C with an incubator shaking horizontally at 100 rpm. The release medium was completely removed and supplemented with fresh PBS at predetermined time intervals. The ART concentration in the medium was recorded with HPLC according to the aforementioned protocol. The cumulative drug release was plotted vs incubation time.

Cellular Uptake of Polymer Micelles

Confocal laser scanning microscopy (CLSM) and flow cytometry were carried out to monitor the intracellular uptake and distribution of drug-conjugated micelles. For CLSM measurements, 1×10^5 CT-26 cells in 500 μL RPMI 1640 were seeded onto glass coverslips which were placed in 6-well plates and incubated for 24 h. Then, the cells were incubated for 0.5 h or 3 h with C_6 or C_6-loaded

prodrug micelles (micelles concentration 50 μg/mL) which were dissolved in 500 μL RPMI 1640 supplemented with 10% FBS. At predetermined time points, the cells nuclei were stained by 10 μg/mL DAPI (Invitrogen, Waltham, MA, USA) for 15 min; then, the cells were washed with cold PBS and fixed with 4% paraformaldehyde. The coverslips were mounted onto glass slides and the cellular uptake was observed using confocal microscopy (Zeiss AXI0, Oberkochen, Germany). For flow cytometry experiments, the cells were first seeded and incubated with different C_6 formulations in the same way as that in the CLSM observations. After incubation, the cells were washed with cold PBS, trypsinized and resuspended in PBS. The suspended cells were directly introduced to a flow cytometer (BD FACS Calibur, San Jose, CA, USA) equipped with a 488 nm argon ion laser.

In Vitro Cytotoxicity and Cell Apoptosis Analysis

To analyze the cytotoxicity of the as-prepared copolymer prodrugs, CT-26 cells were seeded in 96-well plates with a density of 1×10^4 cells per well at 37°C under 5% CO_2 and were subjected to incubation for 24 h. After that, the cells were treated with fresh medium containing blank polymer or polymer prodrugs with concentrations ranging from 1 μM to 1000 μM. After 24 h, 48 h and 72 h of incubation, the cells viability was detected by a microplate reader (Thermo, MK3, Waltham, MA, USA) at an absorbance wavelength of 570 nm using MTT assay, respectively. The cellular viability data were analyzed using GraphPad Prism 5.01.

For cell apoptosis assay, cells were seeded in 12-well plates at 2×10^5 cells/well. After 24 h of incubation, various ART formulations (ART dosage 100 μM) were added to the cells medium and incubated for 24, 48 and 72 h, respectively. Then, the cells were harvested, washed twice with cold PBS and stained with Annexin V-FITC (BD Pharmingen, San Jose, CA, USA) and PI (BD Pharmingen) for 15 min at room temperature under dark. Then, the treated cells were resuspended in PBS and were analyzed by flow cytometry (BD FACS Calibur).

Mitochondrial Membrane Potential Assay

Mitochondrial membrane potential was monitored using JC-1 Assay Kit (Beyotime Biotechnology) under flow cytometry following the manufacturer's recommendations with slight modifications. In brief, cells were seeded in 96-well plates and incubated overnight. Then, the cells were treated with free ART, PBAE-ART4, or PBAE-ART2, respectively, at ART dosage of 100 μM and then incubated for additional 24 h. The change of mitochondrial membrane potential of the cells was detected by incubation with a fluorescent probe JC-1 at 37°C for 15 min. After washing with incubation buffer for three times, the cells were directly analyzed by flow cytometry.

Cellular Reactive Oxygen Species (ROS) Measurements

The released intracellular ROS in different groups was evaluated using 6-carboxy-2′, 7′-dichlorodihydrofluorescein diacetate (DCFHDA, Qayee Bio, Shanghai, China). CT-26 cells were seeded in 96-well plates with a density of 1×10^4 cells/well at 37°C and were incubated for 24 h. Then, the cells were incubated with free ART, PBAE-ART4, or PBAE-ART2 with ART dosage of 100 μM for 24 h, respectively. The cells were collected and resuspended in 10 μM DCFHDA. After incubation at 37°C for 30 min, the fluorescence was measured using a microplate reader (excitation at 485 nm and emission at 530 nm).

Western Blot Analysis

CT-26 cells were seeded in 6-well plates and were incubated with free ART, PBAE-ART4 or PBAE-ART2 (ART dosage 100 μM) for 24 h. Then, the cells were washed with cold PBS twice and incubated with lysis buffer containing 1 mmol phenylmethylsulfonyl fluoride for 30 min. A total of 30.0 μg of the proteins from different samples were added to the 10% SDS–polyacrylamide gel to separate proteins with different molecular weights which were then transferred to the PVDF membrane for 1 h, followed by blocking the membrane using 5% nonfat milk prepared with TBST (Tris buffered saline and Tween 20) solution for 1 h at room temperature and incubation with different primary antibodies of anti-cytochrome c antibody (1:5000 diluted, 14 kDa, Abcam), anti-caspase-3 (1:1000 diluted, 46 kDa, Abcam) and anti-caspase-9 (1:1000 diluted, 32 kDa, Abcam) overnight at 4°C, respectively. Then, the secondary antibodies anti-rabbit IgG (Abcam) and anti-mouse IgG (Abcam) were applied to incubate with the corresponding antibodies for 45 min. After the membrane was washed with TBST for 10 min for three times, the bounded antibodies were detected with enhanced chemiluminescence reagents (Amersham, OH, USA) and the membrane was exposed to hyperfilm (Amersham). The intensities of the proteins were measured by Image J (Tanon 5200) software

and normalized to that of GAPDH and expressed as relative ratios.

In vivo Tumor Inhibition Studies

Six-week female BALB/c mice (Academy of Military Medical Sciences, Beijing, China) were used as animal models. Animal studies were conducted according to the regulation on experimental animals of China Academy of Chinese Medical Sciences (CACMS), and were approved by the animal care and use committee of the Institute of Chinese Materia Medica, CACMS. CT-26 cells were seeded subcutaneously (2×10^7 cells/mouse) into mice. Mice were randomly divided into four groups (n = 5) when the volume of tumors reached near 100 mm^3. The therapeutic effect of ART, PBAE-ART4 and PBAE-ART2 on the xenograft rodent tumor was analyzed by tail vein injection of the respective ART formulations (ART dosage of 20 mg/kg) every 2 days for 5 times, respectively. The body weight and tumor volume were recorded and calculated every 2 days for 3 weeks. Mice were sacrificed at 21st day post-treatment and the primary tumors were excised and weighted. The tumor volume (V) was calculated as follows: $V = (L \times W^2)/2$, where L and W were the longest and the shortest diameter of the tumor.

Statistical Analysis

Data were processed using GraphPad Prism 5.01 software and presented as mean ± standard deviation (SD). Statistical analysis was performed using one-way analysis of variance (ANOVA). The difference was regarded statistically significant as $*P < 0.05$, very significant as $**P < 0.01$, and extremely significant as $***P < 0.001$.

Results

Synthesis and Characterization of Polymers and Polymer Prodrugs

The preparation procedures used in the synthesis of polymer conjugates were depicted in (Scheme 2). The hydrophilic polymer PEOz was synthesized via ring opening polymerization (ROP) of 2-ethyl-2-oxazoline as initiated by Boc-OTs. The polymerization process was quenched by methanolic potassium hydroxide to introduce hydroxyl group at the end of PEOz, which could be further conjugated with poly(D,L-lactide) (PLA) segment by ROP of D,L-lactide with tin octoate as catalyst. Then, the copolymer was further end-caped with poly(β-amino ester) (PBAE) segment by activation of PEOz-PLA with acryloyl chloride and following Michael addition of diacrylate ester and amine groups (Scheme 2). The chemical structures of the copolymers were characterized by ^{1}H NMR ($CDCl_3$, 600 MHz) analysis, with corresponding chemical shifts of the ^{1}H NMR spectra as shown in (Figure S1). δ1.41 (a, Boc-OTs, -O($C\underline{H}_3$)$_3$), 3.38 (b, Boc-OTs, -$OCH_2C\underline{H}_2$-), 4.07 (c, Boc-OTs, -$OC\underline{H}_2CH_2$-), 7.79 (d, Boc-OTs, -C=C$\underline{H}$-CH=C-), 7.35 (e, Boc-OTs, -C=CH-C$\underline{H}$=C-), 2.45 (f, Boc-OTs, =C-C$\underline{H}_3$) (Figure S1A); δ1.76 (a, PEOz, -C-($C\underline{H}_3$)$_3$), 3.46 (b, PEOz, -N-$C\underline{H}_2$-CH_2-), 2.40 (c, PEOz, -C-CH_2-$C\underline{H}_3$), 1.12 (d, PEOz, -C-CH_2-$C\underline{H}_3$) (Figure S1B); δ5.20 (e, PLA, -C$\underline{H}$-) (Figure S1C); δ5.91–6.19 (f, g, acryloyl, =$C\underline{H}_2$) and δ6.47 (h, acryloyl, -O-CO-C$\underline{H}$=) (Figure S1D); δ4.16 (i, bisacrylate, -$C\underline{H}_2$-OC=O), 3.03 (j, N-methenyl, N-C$\underline{H}$-) (Figure S1E). It can be demonstrated that PEOz-PLA-PBAE copolymers were successfully synthesized according to the ^{1}H NMR spectra.

The PBAE-ART prodrugs were synthesized through esterification reaction between PELA-PBAE copolymers and ART. The chemical structures of the copolymer prodrugs were characterized by ^{1}H NMR analysis. The characteristic chemical shift of ART could be easily identified at δ 5.40 (l, artesunate, 1H) and 5.60 (k, artesunate, 1H) (Figure S1F).

The PEOz-PLA-PBAE copolymers could be self-assembled into micelles in aqueous solution. The critical micelle concentration (CMC) of the copolymers was characterized by pyrene fluorescence spectrometry to monitor the self-assembly behavior of the copolymers. It should be noted that the as-prepared copolymers exhibited very low CMC values (Table 1, Figure S2), which is highly desirable when the formulations to be used for intravenous administration. The sizes of the PELA-PBAE-ART micelles increased significantly after conjugation with ART, as compared to that of the PELA-PBAE copolymers, indicating the more rigid molecular structure of the polymer prodrugs due to introduction of the hydrophobic ART molecules into the cores of the amphipathic copolymers (Table 2). The morphology of ART-conjugated micelles was characterized by TEM, which showed spherical morphologies of the micelles (Figure S3). It should be noted that the size measured by TEM was smaller than that characterized by the dynamic light scattering (DLS), which should be ascribed to the shrinkage of the micelle after drying,[37] as compared to the stretching state of the micelle corona in the aqueous solution measured by DLS. Our results demonstrated that the formed polymeric micelles have sizes smaller than 200 nm, which may facilitate the accumulation of the polymer prodrugs in

tumor cells.[38] To further evaluate the influence of pH on the size and surface charge of the polymeric micelles, the as-prepared micelles were exposed to different incubation milieu with pH at 5.0, 5.5, 6.0, 6.5 and 7.4, respectively, and incubated at 37°C to monitor the changes of micelles' size and zeta potential as measured by DLS (Figure S4). It can be observed that the sizes of PELA-PBAE-ART1, PELA-PBAE-ART2 or PELA-PBAE-ART3 micelles increased slightly by decreasing the pH of the incubation medium from 7.4 to 5.0. However, the sizes of PELA-PBAE-ART4, PELA-PBAE-ART5, and PELA-PBAE-ART6 micelles increased dramatically under similar conditions. For example, the size of PELA-PBAE-ART4 micelles increased from 195 nm (pH 7.4) to 320 nm (pH 6.0) and decreased dramatically from 320 nm (pH 6.0) to 205 nm (pH 5.0), which might be ascribed to the protonation of PBAE segment in the pH range from 7.4 to 6.0, leading to the expansion of the micelles sizes due to the electrostatic repulsion of the PBAE molecular chains, which was confirmed by the charge reversal of the synthesized polymer prodrugs in acidic environments (Figure S4A). From pH 6.0 to 5.0, the sizes of the micelles decreased due to the electrostatic screening effect of the excess protons in the surrounding milieu, leading to decreased or diminished electrostatic repulsion between the PBAE chains.[39] As aforementioned, the ζ potentials of the prodrugs increased significantly by decreasing the surrounding pH from 7.4 to 6.5 (Figure S4B), due to the protonation of the PBAE segment, and subsequent partial charge neutralization.[40,41]

The stability of the polymer prodrugs was investigated by measurement of micelles' sizes vs incubation time according to our previous protocol.[35] As shown in Figure S5, the sizes of PELA-PBAE-ART2 prodrug showed high stability in the investigated period, whereas the sizes of other prodrugs increased to some extent during incubation. The drug grafting ratios (GR) of the polymer prodrugs were ranged from 2.14 ±1.08% to 9.57±1.24%, respectively (Table 3), which was in good agreement with the result calculated from the ^{1}H NMR data. The PEOz-PLA-PBAE copolymers were small sized and narrowly distributed. However, significant increase in the micelles' sizes was observed after conjugation of the drug onto the polymers backbone (Table 2). It should be noted that the polymer prodrug (PBAE-ART1 and PBAE-ART4) containing 1,4-butanediol diacrylate groups has higher drug grafting ratio and larger micelle sizes. As a comparison, the copolymer prodrug (PBAE-ART3 and PBAE-ART6) consisting of 1,9-bis(acryloyloxy) nonane groups have lower drug grafting ratio and smaller sizes. Whereas the copolymer PBAE-ART2 consisting of 2-amino-1,3-propanediol and 1,6-hexanediol diacrylate showed high stability during incubation. Therefore, PBAE-ART4 and PBAE-ART2 prodrugs were used in the subsequent in vitro and in vivo studies.

Table 1 Characterization of Poly(2-Ethyl-2-Oxazoline)-Poly (Lactide)-Poly(β-Amino Ester) Copolymers (n=3)

Copolymers	Mn (1H-NMR)*	Mn (GPC) #	PDI	p*Kb*	CMC (mg/L)
PEOz-PLA-PBAE-1	7249	7113	1.10	6.3	2.37
PEOz-PLA-PBAE-2	8293	7406	1.04	6.4	2.38
PEOz-PLA-PBAE-3	7153	6626	1.19	6.5	1.79
PEOz-PLA-PBAE-4	7782	6510	1.21	6.4	2.05
PEOz-PLA-PBAE-5	6985	6570	1.11	6.3	5.01
PEOz-PLA-PBAE-6	6596	6667	1.11	6.3	1.74

Notes: A_1: 2-amino-1,3-propanediol, A_2: 6-amino-1-hexanol, B_1: 1.4-butanediol diacrylate, B_2: 1.6-hexanediol diacrylate, B_3: 1.9-bis(acryloyloxy) nonane. PEOz-PLA-PBAE-1 (A_1B_1), PEOz-PLA-PBAE-2 (A_1B_2), PEOz-PLA-PBAE-3 (A_1B_3) PEOz-PLA-PBAE-4 (A_2B_1), PEOz-PLA-PBAE-5 (A_2B_2), PEOz-PLA-PBAE-6 (A_2B_3). *Characterized by Mn (^{1}H NMR, $CDCl_3$ as solvent, 600 MHz). #GPC (eluent: tetrahydrofuran, flow rate: 0.5 mL/min). The p*Kb* values were determined by acid-base titration. CMC was measured using pyrene fluorescence spectroscopy.

Abbreviations: CMC, critical micelle concentration; GPC, gel permeation chromatography; Mn, number average molecular weight; PDI, Polydispersity index; p*Kb*, Alkaline ionization equilibrium constant; PEOz, poly (2-ethyl-2-oxazoline); PLA, poly (lactic acid); PBAE, poly(β-amino ester).

In Vitro Drug Release

The drug release behavior of ART-conjugated prodrugs was investigated at 37°C in pH 7.4 or pH 6.0, respectively. As

Table 2 Variation of the Sizes of the PEOz-PLA-PBAE Copolymers Before and After Conjugation of ART (n=3)

Copolymers	Size (nm)	PDI	Polymer Prodrugs	Size (nm)	PDI
PEOz-PLA-PBAE-1	152.6±2.5	0.240	PBAE-ART1	190.31±4.5	0.69
PEOz-PLA-PBAE-2	48.3±1.4	0.392	PBAE-ART2	68.78±1.3	0.197
PEOz-PLA-PBAE-3	30.4±0.5	0.558	PBAE-ART3	33.45±0.8	0.214
PEOz-PLA-PBAE-4	148.5±5.9	0.447	PBAE-ART4	197.25±6.4	0.648
PEOz-PLA-PBAE-5	58.2±1.7	0.375	PBAE-ART5	105.50±3.1	0.674
PEOz-PLA-PBAE-6	56.9±2.1	0.248	PBAE-ART6	97.43±2.2	0.537

Table 3 The Grafting Ratio (GR) of ART on the Respective Polymers Prodrugs Determined by HPLC and ^{1}H NMR, Respectively (n=3)

Polymer Prodrugs	GR (HPLC)	GR (1H-NMR)
PBAE-ART1	5.31%±0.25%	6.43%
PBAE-ART2	4.96%±0.18%	7.12%
PBAE-ART3	3.98%±0.59%	5.74%
PBAE-ART4	9.57%±1.24%	10.2%
PBAE-ART5	3.79%±0.29%	5.52%
PBAE-ART6	2.14%±1.08%	3.65%

shown in Figure S6, similar release profiles of PBAE-ART4 and PBAE-ART2 micelles were observed at pH 7.4 and pH 6.0, respectively, with 57.2% and 55.9% of the drug released from the PBAE-ART4 and PBAE-ART2 micelles after 48 h incubation at pH 7.4, respectively. However, 91.4% and 92.8% of ART was released from PBAE-ART4 and PBAE-ART2 micelles at pH 6.0 within 48 h.

In Vitro Cellular Uptake

Coumarin-6 (C_6) was employed as a model drug to investigate the cellular internalization of the as-prepared polymer prodrugs. The uptake of PBAE-ART4-C_6 or PBAE-ART2-C_6 micelles by CT-26 cells was observed by confocal laser scanning microscopy (CLSM) and flow cytometry. As shown in (Figure 1A), only weak fluorescence in the cytoplasm was observed after incubation with free C_6 for 3 h. As a comparison, stronger fluorescence in the cytoplasm was illuminated in the cells incubated with PBAE-ART4-C_6 or PBAE-ART2-C_6 micelles. The flow cytometry analysis also demonstrated significant improvement of the fluorescence in the micellar groups, as compared to that of the free fluorescent probe, demonstrating enhanced cellular uptake of PBAE-ART4 and PBAE-ART2 micelles than that of free C_6 (Figure 1B). Moreover, the fluorescence of PBAE-ART2-C_6 micelles internalized by the cells was significantly stronger than that of PBAE-ART4-C_6 micelles, indicating the improved internalization of smaller sized micelles by CT-26 cells.

Cytotoxicity Assay and Cellular Apoptosis Analysis

The in vitro cytotoxicity of free ART, PBAE-ART4 and PBAE-ART2 was evaluated by the MTT assay. Dose and time-dependent manner was observed in the cytotoxicity analysis of free ART and ART prodrugs (Figure S7), respectively, which was in accordance with previous studies.[42] The ART-conjugated prodrugs were demonstrated with stronger cytotoxicity against CT-26 cells, as a comparison to that of free ART. As can be seen in Table 4, the IC_{50} of PBAE-ART2 and PBAE-ART4 micelles were 1.94 fold and 1.37 fold lower than that of free ART after incubation for 72 h, respectively, indicating the stronger inhibitory efficacy of the PBAE-ART2 micelles against CT-26 cells.

Annexin V/PI staining was carried out to investigate the influence of the apoptosis rates on CT-26 cells of various ART formulations. The apoptosis rates for cells treated with free ART, PBAE-ART4 and PBAE-ART2 for 24 h were 8.76%, 11.88% and 14.27%, respectively. After incubation for 72 h, the apoptosis rates were increased to 18.41%, 22.49% and 26.85%, respectively, with stronger apoptosis rates were observed in the micelles groups than that of free drug (Figure 2). Moreover, an improved inhibitory activity of PBAE-ART2 against that of PBAE-ART4 was observed due to the enhanced cellular uptake of the PBAE-ART2 prodrug (Figure 1A).

Mitochondrial Membrane Potentials and Cellular ROS Analysis

CT-26 cells were harvested and stained with JC-1, and subjected to flow cytometry analysis to determine the loss of mitochondrial membrane potential (Δψm). The JC-1 probe concentrates in the mitochondria with intact mitochondrial membrane (high membrane potentials) as red fluorescent aggregates, which will be released into cytoplasm in the state of monomers with green fluorescence when the permeability of mitochondria membrane increases (low membrane potentials). Therefore, the red/green fluorescence ratio in the cells was measured to demonstrate the loss of mitochondrial membrane potential (Δψm) in this study. Our results demonstrated that the Δψm of CT-26 cells decreased significantly (1.85 fold and 14.75 fold) after incubation with PBAE-ART4 and PBAE-ART2 (Figure 3A) for 72 h, respectively, with a comparison to free ART.

The formation of intracellular ROS in CT-26 colon cancer cells was further measured after incubation with different ART formulations (Figure 3B). It has been shown that the intracellular ROS levels in the PBAE-ART4 and PBAE-ART2 groups increased 1.43 fold and 1.83 fold, respectively, as compared with free ART group.

Western Blot Analysis

The apoptosis of CT-26 cells was investigated by Western blotting analysis after incubation of the cells with various ART formulations. It has been reported that cytochrome

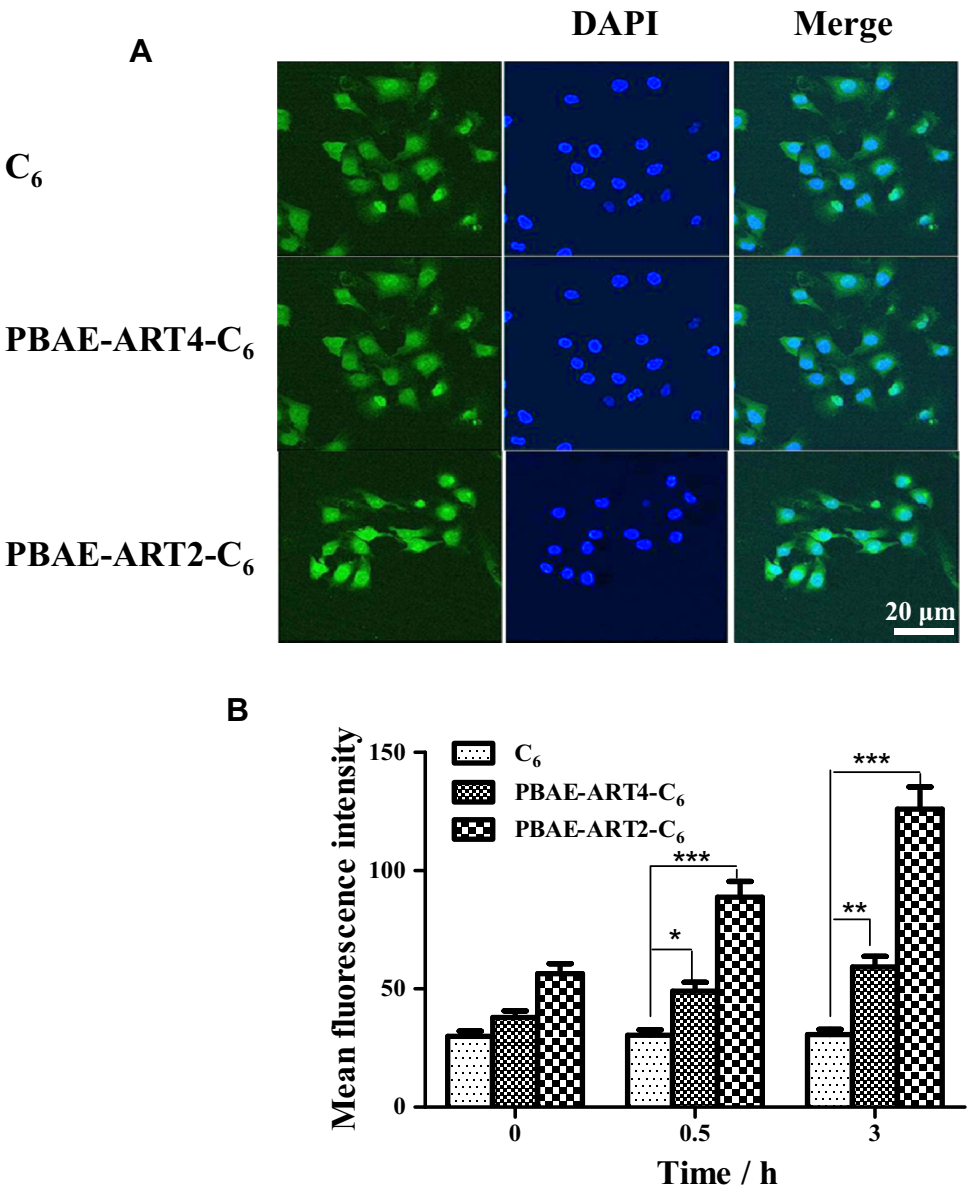

Figure 1 Cellular uptake of free C_6 and micelles incorporated C_6. (**A**) Confocal FL images of cellular internalized C_6, PBAE-ART4-C_6 and PBAE-ART2-C_6, after 3 h incubation with CT-26 cells. Blue FL represents DAPI, green FL represents C_6. (**B**) Flow cytometry analysis of mean FL intensity (n=10,000 cells) in CT-26 cells incubated with C_6, PBAE-ART4-C_6 and PBAE-ART2-C_6 for 0.5 h and 3 h, respectively. Data are presented as the mean of three measurements ± SD. *P<0.05, **P<0.01, ***P<0.001.

c may upregulate the expression of caspase 9 as well as caspase 3 in the mitochondrial apoptosis pathway.[43] It was illustrated that the expression of apoptosis-associated proteins such as cytochrome c, caspase 9 and caspase 3 increased significantly after CT-26 cells were treated by PBAE-ART4 and PBAE-ART2, respectively, as compared to the free drug (Figure 4).

In vivo Tumor Inhibition Studies

In the current study, rodent CT-26 xenograft tumor model was established to evaluate the anticancer efficacy of various ART formulations on BALB/c mice via intravenous administration. As shown in Figure 5A, significant difference in the tumor volume of various therapeutic groups can be observed. The tumor volumes were 542.5, 690.5 and 727.8 mm^3 in PBAE-ART2, PBAE-ART4 and ART group in the 21st day post-treatment, respectively, as compared to 834.9 mm^3 of the saline group, indicating enhanced inhibitory effect of the as-prepared prodrugs. No significant difference in the body weight of mice was observed in the various ART formulations, demonstrating its high biocompatibility of the polymer prodrugs (Figure 5B). On the other hand, PBAE-ART2 showed better efficacy than that of

Table 4 The Half Inhibition Concentration (IC_{50}) of Different ART Formulations on CT-26 Cells After Incubation for 24, 48 and 72 h, Respectively

Drug Formulation	IC_{50}(μM)		
	24h	48h	72h
ART	247.9±18.86	219.3±29.45	103.2±4.18
PBAE-ART4	157.7±23.63	129.9±18.88	75.31±4.07
PBAE-ART2	91.76±14.92	83.94±1.806	53.31±8.74

PBAE-ART4 (Figure 5C), hinting the pH-sensitive PBAE-ART2 prodrug may promote the accumulation of the anticancer drug in tumor cells, which is consistent with the confocal microscopy experiments (Figure 1A).

Immunohistochemical Analysis

The therapeutic efficacy of the ART prodrugs was confirmed again by histological analysis. As shown in Figure 6, tissue necrosis and vacuolization could be observed in tumor tissues after treatment with various ART formulations, as compared with control group. Moreover, the ART prodrugs showed better inhibitory efficacy on the xenograft tumor, which may be ascribed to the enhanced penetration of the polymer conjugated prodrugs into tumors.

Discussion

The number average molecular weight (Mn) of the copolymers was characterized by ^{1}H NMR and gel permeation chromatography (GPC). It can be seen that the as-prepared copolymers were narrowly distributed with Mn (GPC) slightly less than Mn (NMR), which may be ascribed to the different chemical structure of polystyrene (PS) used for calibration of the molecular weight of the triblock copolymers by GPC (Table 1).

The synthesized PEOz-PLA-PBAE copolymers exhibited a sharp pH change in the pH range from 4 to 10 (Figure S8), suggesting the pH-sensitive characteristics of the copolymers. The p*K*b values of the copolymers with different structures ranged from 6.3 to 6.5, as shown in Table 1 and Figure S8. It has been reported that most solid tumors exhibited weak acid environment,[44] with even lower pH values observed in the organelles of tumor cells.[45] The pH-triggered release of the drug from the nano-drug carriers plays an important role in their applications in tumor therapy.[46] It would be highly desirable to release the conjugated drug rapidly in the mild acidic tumor environment.[47] The current study demonstrated the accelerated drug release of the polymer prodrugs under mild acidic conditions, which could be ascribed to hydrophobic/hydrophilic transition of the PBAE block at lower pH values due to the protonation of the amino groups,[47] resulting in the stretching state of ART linked PBAE chains and accelerated release of the conjugated drug.[48] It should be noted that no significant difference was observed in the drug release profiles of PBAE-ART4 and

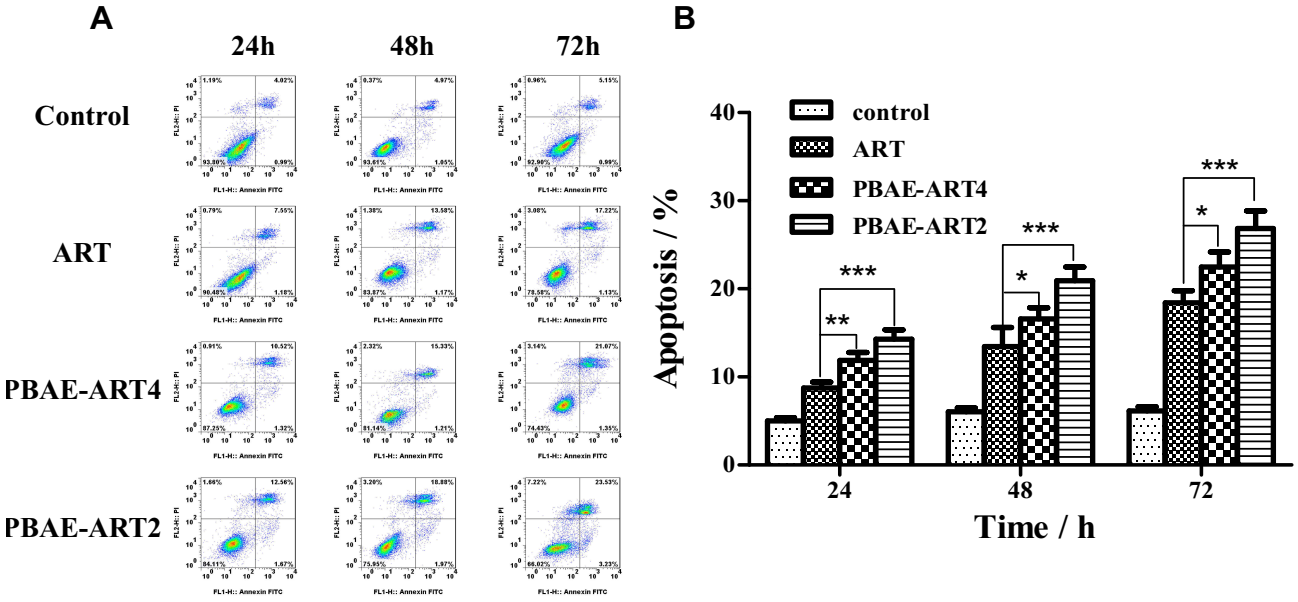

Figure 2 The apoptosis rates of CT-26 cells after incubation with various ART formulations. (**A**) Flow cytometry analysis via Annexin V/PI staining, (**B**) Quantitative analysis of tumor cells apoptosis after incubation with ART formulations for 24, 48 and 72 h, respectively. *P<0.05, **P<0.01, ***P<0.001.

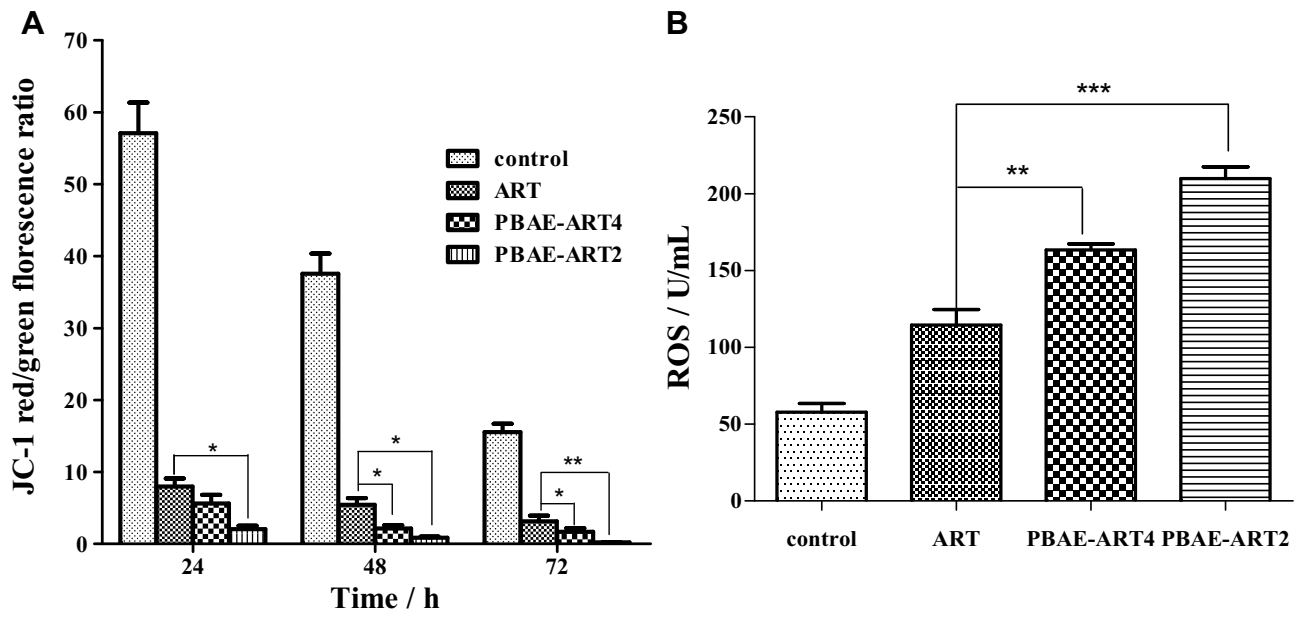

Figure 3 (**A**) The decrease of mitochondrial membrane potential after incubation of CT-26 cells with ART formulations for 24, 48 and 72 h, respectively. (**B**) The increased ROS level in CT-26 cells after challenge with various ART drugs. *P<0.05, **P<0.01, ***P<0.001.

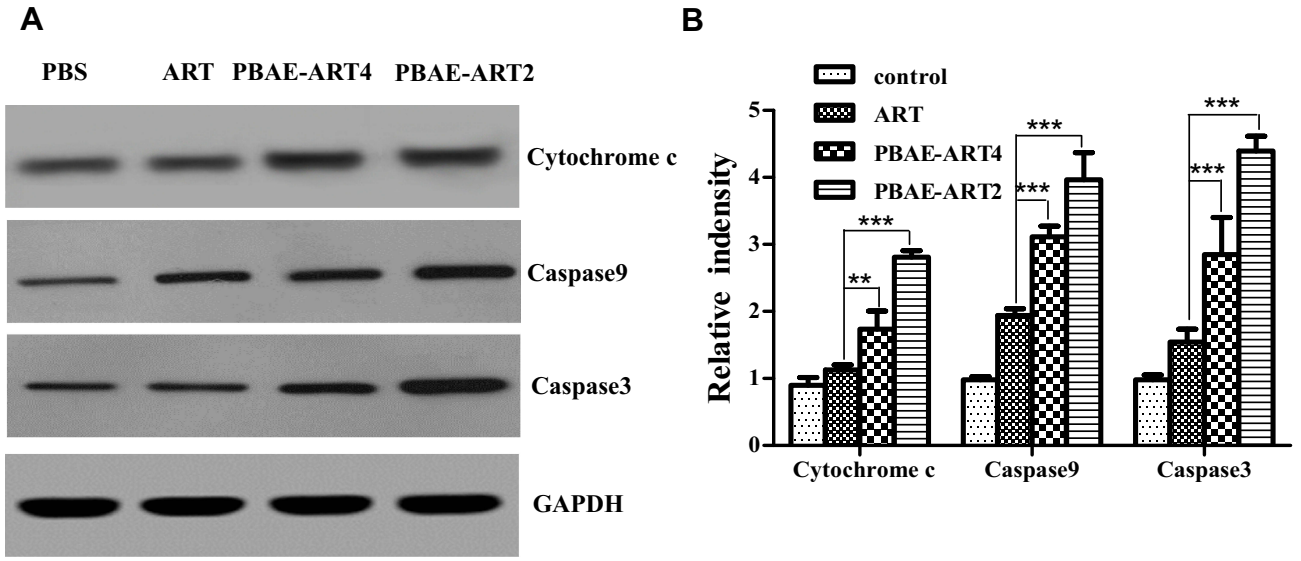

Figure 4 Western blotting analyses of CT-26 cells after incubation with various ART formulations for 24 h. (**A**) The expression of cytochrome c, caspase 9 and caspase 3 in CT-26 cells, GAPDH as control, (**B**) Relative intensities of the expression of the proteins in the cells. **P<0.01, ***P<0.001.

PBAE-ART2 micelles, which might be ascribed to the similar chemical structure of the two prodrugs.

The mitochondria play a critical role in cell metabolism, homeostasis and apoptosis, as well as cellular autophagy.[49,50] The enhanced permeability of mitochondrial membrane (or loss of mitochondrial membrane potential) is a marker event in the process of cellular apoptosis.[51] In this study, the mitochondrial membrane potential of CT-26 cells decreased significantly after incubation with ART prodrugs, as compared to that of free ART (Figure 3A). It can be hypothesized that the ART prodrug may trigger mitochondrial apoptotic pathway in CT-26 cells. Moreover, a significant decrease of ROS level was observed in the cells treated with ART prodrugs (Figure 3B). It has been shown that intracellular ROS plays an important role in cell death by inducing apoptosis.[52] The excessive ROS may induce oxidative stress on mitochondria and destruction of the integrity of the mitochondria membrane structure, and induce

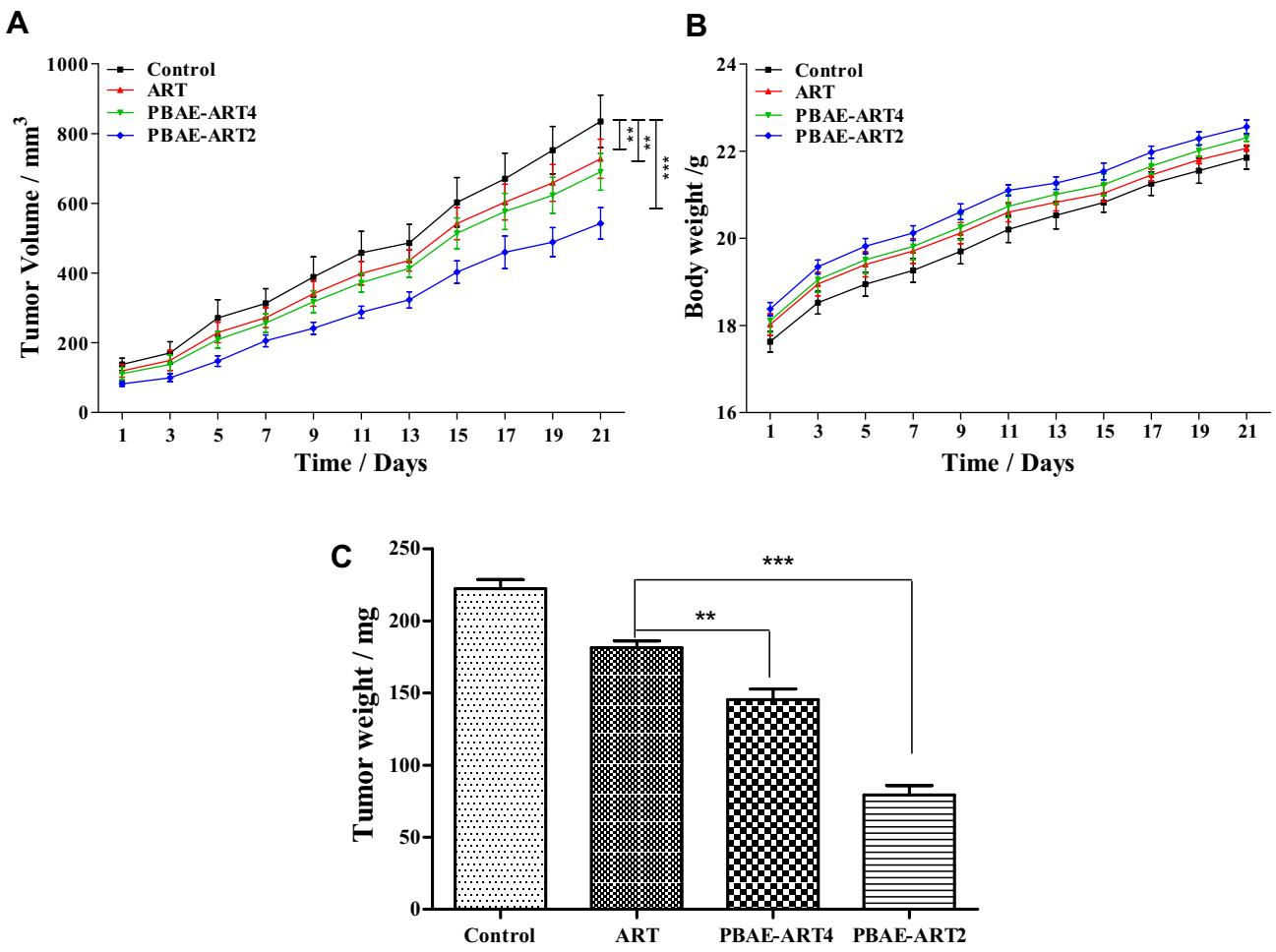

Figure 5 In vivo tumor inhibitory effects of various ART formulations on CT-26 xenograft tumors. (**A**) The tumor volume of CT-26 tumors post-treatment by ART formulations via *i.v.* administration, (**B**) The body weight of mice in various groups post-treatments, (**C**) Weight of tumors of each therapeutic group on the 21st day post-therapy. ***P*<0.01, ****P*<0.001.

accelerated release of cytochrome c for activation of cellular apoptosis.[53] It has been indicated that the ART-conjugated prodrugs were more effective in induction of ROS than that of free ART, which may be ascribed to the elongated half-life (data not shown) and the sustained release manner of the prodrugs.[6]

It was demonstrated that the ART-conjugated prodrugs showed higher potency in upregulation of apoptosis-associated proteins and promotion of the apoptosis of CT-26 cells (Figure 4). It was revealed that the released cytochrome c can bind to Apaf, and the formed cytochrome c/Apaf complex can activate the expression of caspase-9, which activates the downstream caspase-3 for induction of apoptosis in CT-26 cell lines.[54]

It has been reported that nano-sized drug delivery systems are advantageous in tumor therapy with prolonged drug circulation time and enhanced accumulation of drug in tumor tissues.[46] Zhang et al reported a pH-responsive artemisinin dimer in lipid nanoparticles showing enhanced anti-tumor efficacy against xenograft tumor.[55] In this study, the in vivo anti-tumoral effect of the ART prodrugs was analyzed on CT-26 xenograft tumor-bearing mice. As can be seen in Figure 5, the pH-responsive polymer prodrugs showed significant inhibitory efficacy on the growth of tumors through the enhanced cellular uptake of the drug depot by the cancer cells (Figure 1), which was consistent with our previous studies.[35] The histopathological analysis also confirmed the elevated therapeutic effect of the polymeric micelles by promoting apoptosis of CT-26 cells.

Conclusion

In this study, artesunate was conjugated with pH-sensitive poly(2-ethyl-2-oxazoline)-poly(lactic acid)-poly(β-amino ester) triblock copolymers for accumulated delivery of the drug to tumor cells and pH stimulated drug release under tumor acidic microenvironment. The enhanced

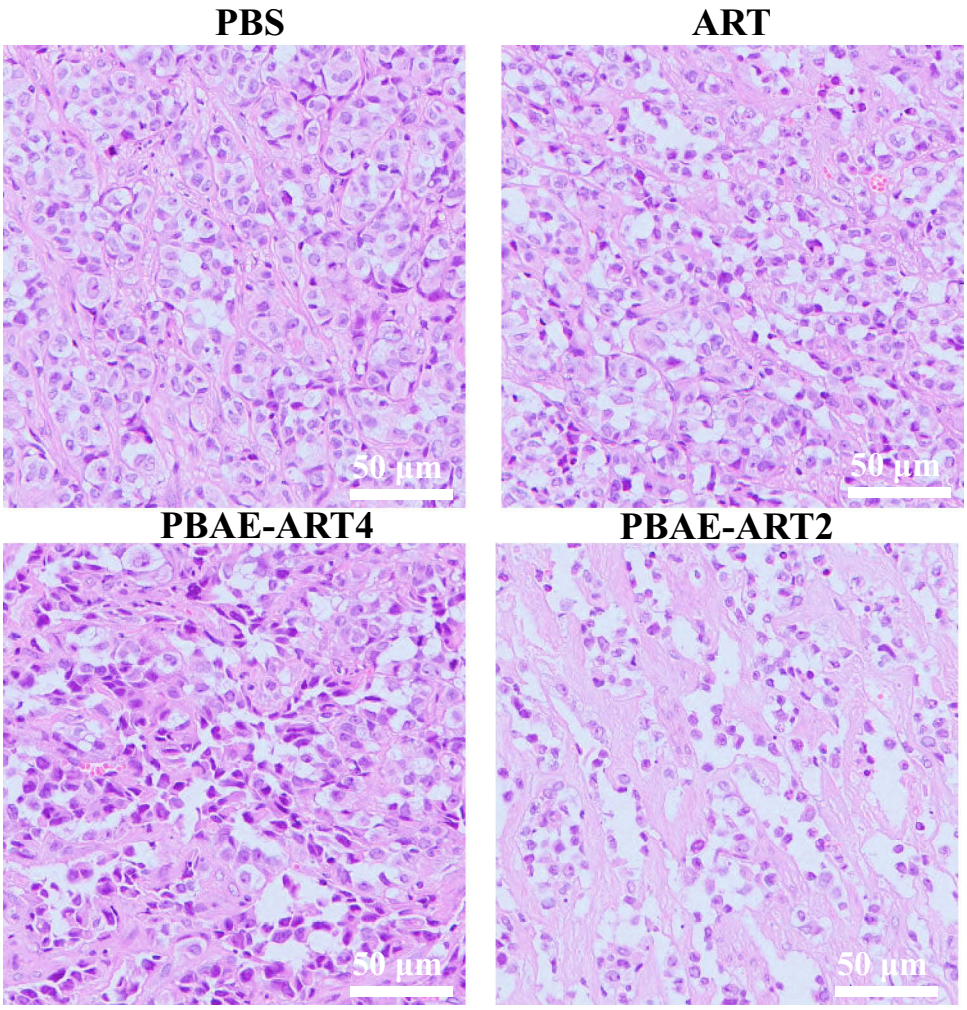

Figure 6 Histopathology analyses of tumor tissues of BALB/c mice in different ART formulation groups.

internalization of the pH-responsive polymer micelles was confirmed by CLSM. The ART prodrugs showed better efficacy in induction of apoptosis of CT-26 cells, as reflected by flow cytometry analysis. The prodrug PBAE-ART2 showed better antitumor effect through the induction of ROS production, and the enhanced expression of tumor apoptosis-associated proteins, as compared with the free drug. The efficacy of ART prodrugs was also confirmed at animal level with a rodent colon cancer model. Results showed the as-prepared ART prodrugs exhibited high potential for colon cancer adjuvant therapy.

Acknowledgments

This study was financially supported by Natural Science Foundation of China (81974461), National S&T Major Project of China (No. 2018ZX09201011), and Natural Science Foundation of Beijing Municipality (2192060).

Disclosure

The authors report no conflicts of interest in this work.

References

1. Bray F, Ferlay J, Soerjomataram I, et al. Global cancer statistics 2018: GLOBOCAN estimates of incidence and mortality worldwide for 36 cancers in 185 countries. *CA Cancer J Clin*. 2018;68(6):394–424. doi:10.3322/caac.21492
2. McQuade RM, Stojanovska V, Bornstein JC, Nurgali K. Colorectal cancer chemotherapy: the evolution of treatment and new approaches. *Curr Med Chem*. 2017;24(15):1537–1557. doi:10.2174/0929867324666170111152436
3. Ma LP, Qin CL, Wang MC, et al. Preparation, preliminary characterization and inhibitory effect on human colon cancer HT-29 cells of an acidic polysaccharide fraction from Stachys floridana Schuttl. ex Benth. *Food Chem Toxicol*. 2013;60:269–276. doi:10.1016/j.fct.2013.07.060
4. Kemeny NE. Treatment of metastatic colon cancer: "the times they are A-changing". *J Clin Oncol*. 2013;31(16):1913–1916. doi:10.1200/JCO.2013.49.4500
5. Coghlin C, Murray GI. Biomarkers of colorectal cancer: recent advances and future challenges. *Proteom Clin Appl*. 2015;9(1–2):64–71. doi:10.1002/prca.201400082

6. Lu L, Kanwar J, Schmitt S, et al. Inhibition of tumor cellular proteasome activity by triptolide extracted from the Chinese medicinal plant 'thunder god vine'. *Anticancer Res*. 2011;31(1):1–10.
7. Efferth T, Kaina B. Toxicity of the antimalarial artemisinin and its derivatives. *Crit Rev Toxicol*. 2010;40(5):405–421. doi:10.3109/10408441003610571
8. Du JH, Zhang HD, Ma ZJ, Ji KM. Artesunate induces oncosis-like cell death in vitro and has antitumor activity against pancreatic cancer xenografts in vivo. *Cancer Chemother Pharmacol*. 2010;65(5):895–902. doi:10.1007/s00280-009-1095-5
9. Papanikolaou X, Johnson S, Garg T, et al. Artesunate overcomes drug resistance in multiple myeloma by inducing mitochondrial stress and non-caspase apoptosis. *Oncotarget*. 2014;5(12):4118–4128. doi:10.18632/oncotarget.1847
10. Zhou HJ, Wang WQ, Wu GD, Lee J, Li A. Artesunate inhibits angiogenesis and downregulates vascular endothelial growth factor expression in chronic myeloid leukemia K562 cells. *Vasc Pharmacol*. 2007;47(2–3):131–138. doi:10.1016/j.vph.2007.05.002
11. Zuo W, Wang ZZ, Xue J. Artesunate induces apoptosis of bladder cancer cells by miR-16 regulation of COX-2 expression. *Int J Mol Sci*. 2014;15(8):14298–14312. doi:10.3390/ijms150814298
12. Chen K, Shou LM, Lin F, et al. Artesunate induces G2/M cell cycle arrest through autophagy induction in breast cancer cells. *Anti-Cancer Drug*. 2014;25(6):652–662. doi:10.1097/CAD.0000000000000089
13. Roh JL, Kim EH, Jang H, Shin D. Nrf2 inhibition reverses the resistance of cisplatin-resistant head and neck cancer cells to artesunate-induced ferroptosis. *Redox Biol*. 2017;11:254–262. doi:10.1016/j.redox.2016.12.010
14. Pang YL, Qin GQ, Wu LP, Wang XP, Chen TS. Artesunate induces ROS-dependent apoptosis via a Bax-mediated intrinsic pathway in Huh-7 and Hep3B cells. *Exp Cell Res*. 2016;347(2):251–260. doi:10.1016/j.yexcr.2016.06.012
15. Xu G, Zou WQ, Du SJ, Wu MJ, Xiang TX, Luo ZG. Mechanism of dihydroartemisinin-induced apoptosis in prostate cancer PC3 cells: an iTRAQ-based proteomic analysis. *Life Sci*. 2016;157:1–11. doi:10.1016/j.lfs.2016.05.033
16. Riganti C, Doublier S, Viarisio D, et al. Artemisinin induces doxorubicin resistance in human colon cancer cells via calcium-dependent activation of HIF-1α and P-glycoprotein overexpression. *Br J Pharmacol*. 2009;156(7):1054–1066. doi:10.1111/j.1476-5381.2009.00117.x
17. Greenshields AL, Shepherd TG, Hoskin DW. Contribution of reactive oxygen species to ovarian cancer cell growth arrest and killing by the anti-malarial drug artesunate. *Mol Carcinog*. 2017;56(1):75–93. doi:10.1002/mc.22474
18. Ma H, Yao Q, Zhang AM, et al. The effects of artesunate on the expression of EGFR and ABCG2 in A549 human lung cancer cells and a xenograft model. *Molecules*. 2011;16(12):10556–10569. doi:10.3390/molecules161210556
19. Li PC, Lam E, Roos WP, Zdzienicka MZ, Kaina B, Efferth T. Artesunate derived from traditional Chinese medicine induces DNA damage and repair. *Cancer Res*. 2008;68(11):4347–4351. doi:10.1158/0008-5472.CAN-07-2970
20. Sertel S, Eichhorn T, Sieber S, et al. Factors determining sensitivity or resistance of tumor cell lines towards artesunate. *Chem Biol Interact*. 2010;185(1):42–52. doi:10.1016/j.cbi.2010.02.002
21. Efferth T. Cancer combination therapy of the sesquiterpenoid artesunate and the selective EGFR-tyrosine kinase inhibitor erlotinib. *Phytomedicine*. 2017;37:58–61. doi:10.1016/j.phymed.2017.11.003
22. Bu L, Zhang H, Xu K, Du B, Zhu C, Li Y. pH and reduction dual-responsive micelles based on novel polyurethanes with detachable poly(2-ethyl-2-oxazoline) shell for controlled release of doxorubicin. *Drug Deliv*. 2019;26(1):300–308. doi:10.1080/10717544.2019.1580323
23. Kumar R, Singh M, Meena J, et al. Hyaluronic acid - dihydroartemisinin conjugate: synthesis, characterization and in vitro evaluation in lung cancer cells. *Int J Biol Macromol*. 2019;133:495–502. doi:10.1016/j.ijbiomac.2019.04.124
24. Ismail M, Du Y, Ling L, Li X. Artesunate-heparin conjugate based nanocapsules with improved pharmacokinetics to combat malaria. *Int J Pharm*. 2019;562:162–171. doi:10.1016/j.ijpharm.2019.03.031
25. Liu L, Liu Y, Ma L, et al. Artemisinin-loaded mesoporous nanoplatform for pH-responsive radical generation synergistic tumor theranostics. *ACS Appl Mater Interfaces*. 2018;10(7):6155–6167. doi:10.1021/acsami.7b18320
26. Liu R, Yu X, Su C, Shi Y, Zhao L. Nanoparticle delivery of artesunate enhances the anti-tumor efficiency by activating mitochondria-mediated cell apoptosis. *Nanoscale Res Lett*. 2017;12(1):403. doi:10.1186/s11671-017-2169-7
27. Tong HY, Wang Y, Lu XC, et al. On the preparation of transferrin modified artesunate nanoliposomes and their glioma-targeting treatment in-vitro and in-vivo. *Int J Clin Exp Med*. 2015;8(12):22045–22052.
28. Jin M, Shen X, Zhao C, et al. In vivo study of effects of artesunate nanoliposomes on human hepatocellular carcinoma xenografts in nude mice. *Drug Deliv*. 2013;20(3–4):127–133. doi:10.3109/10717544.2013.801047
29. Craciun I, Gunkel-grabole G, Belluati A, Palivan CG, Meier W. Expanding the potential of MRI contrast agents through multifunctional polymeric nanocarriers. *Nanomedicine (Lond)*. 2017;12(7):811–817. doi:10.2217/nnm-2016-0413
30. Moreira AF, Rodrigues CF, Reis CA, Costa EC, Ferreira P, Correia IJ. Development of poly-2-ethyl-2-oxazoline coated gold-core silica shell nanorods for cancer chemo-photothermal therapy. *Nanomedicine (Lond)*. 2018;13(20):2611–2627. doi:10.2217/nnm-2018-0179
31. Sinha VR, Bansal K, Kaushik R, Kumria R, Trehan A. Poly-ϵ-caprolactone microspheres and nanospheres: an overview. *Int J Pharm*. 2004;278(1):1–23. doi:10.1016/j.ijpharm.2004.01.044
32. Gao Y, Huang JY, O'Keeffe Ahern J, et al. Highly branched poly(β-amino esters) for non-viral gene delivery: high transfection efficiency and low toxicity achieved by increasing molecular weight. *Biomacromolecules*. 2016;17(11):3640–3647. doi:10.1021/acs.biomac.6b01120
33. Clamme JP, Krishnamoorthy G, Mely Y. Intracellular dynamics of the gene delivery vehicle polyethylenimine during transfection: investigation by two-photon fluorescence correlation spectroscopy. *Biochim Biophys Acta*. 2003;1617(1–2):52–61. doi:10.1016/j.bbamem.2003.09.002
34. Maeda H, Wu J, Sawa T, Matsumura Y, Hori K. Tumor vascular permeability and the EPR effect in macromolecular therapeutics: a review. *J Control Release*. 2000;65(1–2):271–284. doi:10.1016/s0168-3659(99)00248-5
35. Chen YJ, Yue QX, De GJ, et al. Inhibition of breast cancer metastasis by paclitaxel-loaded pH responsive poly(β amino ester) copolymer micelles. *Nanomedicine (Lond)*. 2017;12(2):147–164. doi:10.2217/nnm-2016-0335
36. Gong CY, Wang C, Wang YJ, et al. Efficient inhibition of colorectal peritoneal carcinomatosis by drug loaded micelles in thermosensitive hydrogel composites. *Nanoscale*. 2012;4(10):3095–3104. doi:10.1039/c2nr30278k
37. Su X, Ma BX, Hu J, et al. Dual-responsive doxorubicin-conjugated polymeric micelles with aggregation-induced emission active bioimaging and charge conversion for cancer therapy. *Bioconjug Chem*. 2018;29(12):4050–4061. doi:10.1021/acs.bioconjchem.8b00671
38. Cabral H, Matsumoto Y, Mizuno K, et al. Accumulation of sub-100 nm polymeric micelles in poorly permeable tumours depends on size. *Nat Nanotechnol*. 2011;6(12):815–823. doi:10.1038/nnano.2011.166
39. Tong CH, Vilgis TA. Enhanced orientational ordering of water dipoles in uniaxially stretched hydrogels. *J Phys Chem B*. 2008;112(51):16490–16496. doi:10.1021/jp8073943
40. Cheng W, Liang CY, Xu L, et al. TPGS-functionalized polydopamine-modified mesoporous silica as drug nanocarriers for enhanced lung cancer chemotherapy against multidrug resistance. *Small*. 2017;13:29. doi:10.1002/smll.201700623

41. Nie JP, Cheng W, Peng YM, et al. Co-delivery of docetaxel and bortezomib based on a targeting nanoplatform for enhancing cancer chemotherapy effects. *Drug Deliv*. 2017;24(1):1124–1138. doi:10.1080/10717544.2017.1362677
42. Chernysh S, Irina K, Irina A. Anti-tumor activity of immunomodulatory peptide alloferon-1 in mouse tumor transplantation model. *Int Immunopharmacol*. 2012;12(1):312–314. doi:10.1016/j.intimp.2011.10.016
43. Ganguli A, Choudhury D, Datta S, Bhattacharya S, Chakrabarti G. Inhibition of autophagy by chloroquine potentiates synergistically anti-cancer property of artemisinin by promoting ROS dependent apoptosis. *Biochimie*. 2014;107:338–349. doi:10.1016/j.biochi.2014.10.001
44. Barar J, Omidi Y. Dysregulated pH in tumor microenvironment checkmates cancer therapy. *BioImpacts*. 2013;3(4):149–162. doi:10.5681/bi.2013.036
45. Mellman I, Fuchs R, Helenius A. Acidification of the endocytic and exocytic pathways. *Annu Rev Biochem*. 1986;55(1):663–700. doi:10.1146/annurev.bi.55.070186.003311
46. Ulbrich K, Etrych T, Chytil P, Jelínková M, Říhová B. HPMA copolymers with pH-controlled release of doxorubicin: in vitro cytotoxicity and in vivo antitumor activity. *J Control Release*. 2003;87(1–3):33–47. doi:10.1016/s0168-3659(02)00348-6
47. Wang DS, Zhou YX, Li XR, et al. Mechanisms of pH-sensitivity and cellular internalization of PEOz-b-PLA micelles with varied hydrophilic/hydrophobic ratios and intracellular trafficking routes and fate of the copolymer. *ACS Appl Mater Interfaces*. 2017;9(8):6916–6930. doi:10.1021/acsami.6b16376
48. Zhao Y, Zhou YX, Wang DS, et al. pH-responsive polymeric micelles based on poly(2-ethyl-2-oxazoline)-poly(D,L-lactide) for tumor-targeting and controlled delivery of doxorubicin and P-glycoprotein inhibitor. *Acta Biomater*. 2015;17:182–192. doi:10.1016/j.actbio.2015.01.010
49. Galluzzi L, Morselli E, Kepp O, et al. Mitochondrial gateways to cancer. *Mol Aspects Med*. 2010;31(1):1–20. doi:10.1016/j.mam.2009.08.002
50. Mohamed MS, Bishr MK, Almutairi FM, Ali AG. Inhibitors of apoptosis: clinical implications in cancer. *Apoptosis*. 2017;22(12):1487–1509.
51. Caino MC, Altieri DC. Molecular pathways: mitochondrial reprogramming in tumor progression and therapy. *Clin Cancer Res*. 2016;22(3):540–545. doi:10.1158/1078-0432.CCR-15-0460
52. Lu M, Sun LHR, Zhou J, Yang J. Dihydroartemisinin induces apoptosis in colorectal cancer cells through the mitochondria-dependent pathway. *Tumor Biol*. 2014;35(6):5307–5314. doi:10.1007/s13277-014-1691-9
53. Hayashi G, Cortopassi G. Oxidative stress in inherited mitochondrial diseases. *Free Radic Biol Med*. 2015;88(Pt A):10–17. doi:10.1016/j.freeradbiomed.2015.05.039
54. Perkins CL, Fang G, Kim CN, Bhalla KN. The role of Apaf-1, caspase-9, and bid proteins in etoposide- or paclitaxel-induced mitochondrial events during apoptosis. *Cancer Res*. 2000;60(6):1645–1653.
55. Zhang YT, Zhan X, Wang L, Ho RJ, Sasaki T. pH-responsive artemisinin dimer in lipid nanoparticles are effective against human breast cancer in a xenograft model. *J Pharm Sci*. 2015;104(5):1815–1824. doi:10.1002/jps.24407